

## Titanium Dioxide (P25) Produces Reactive Oxygen Species in Immortalized Brain Microglia (BV2): Implications for Nanoparticle Neurotoxicity<sup>†</sup>

THOMAS C. LONG,<sup>‡</sup> NAVID SALEH,<sup>§</sup>  
ROBERT D. TILTON,<sup>||</sup> GREGORY V.  
LOWRY,<sup>§</sup> AND BELLINA VERONESI<sup>\*·‡</sup>

*Department of Environmental Sciences and Engineering, School of Public Health, University of North Carolina, Chapel Hill, North Carolina 27599-7431, Department of Civil and Environmental Engineering, Department of Chemical Engineering, and Department of Biomedical Engineering, Carnegie Mellon University, Pittsburgh, Pennsylvania, 15213, Neurotoxicology Division, National Health and Environmental Effects Research Laboratory, U.S. Environmental Protection Agency, Research Triangle Park, North Carolina, 27711*

Concerns with the environmental and health risk of widely distributed, commonly used nanoparticles are increasing. Nanosize titanium dioxide (TiO<sub>2</sub>) is used in air and water remediation and in numerous products designed for direct human use and consumption. Its effectiveness in deactivating pollutants and killing microorganisms relates to photoactivation and the resulting free radical activity. This property, coupled with its multiple potential exposure routes, indicates that nanosize TiO<sub>2</sub> could pose a risk to biological targets that are sensitive to oxidative stress damage (e.g., brain). In this study, brain microglia (BV2) were exposed to a physico-chemically characterized (i.e., dispersion stability, particle size distribution, and zeta potential) nanomaterial, Degussa P25, and cellular expressions of reactive oxygen species were measured with fluorescent probes. P25's zeta potentials, measured in cell culture media and physiological buffer were  $-11.6 \pm 1.2$  mV and  $-9.25 \pm 0.73$  mV, respectively. P25 aggregation was rapid in both media and buffer with the hydrodynamic diameter of stable P25 aggregates ranging from 826 nm to 2368 nm depending on the concentration. The biological response of BV2 microglia to noncytotoxic (2.5–120 ppm) concentrations of P25 was a rapid (<5 min) and sustained (120 min) release of reactive oxygen species. The time course of this release suggested that P25 not only stimulated the immediate "oxidative burst" response in microglia but also interfered with mitochondrial energy production. Transmission

\* Corresponding author phone: (919) 541-5780; fax: (919) 541-4849; e-mail: veronesi.bellina@epa.gov.

<sup>†</sup> This paper is part of a focus group on Effects of Nanomaterials.

<sup>‡</sup> University of North Carolina.

<sup>§</sup> Department of Civil and Environmental Engineering, Carnegie Mellon University.

<sup>||</sup> Department of Chemical Engineering and Department of Biomedical Engineering, Carnegie Mellon University.

<sup>‡</sup> U.S. Environmental Protection Agency.

electron microscopy indicated that small groups of nanosized particles and micron-sized aggregates were engulfed by the microglia and sequestered as intracytoplasmic aggregates after 6 and 18 h exposure to P25 (2.5 ppm). Cell viability was maintained at all test concentrations (2.5–120 ppm) over the 18 h exposure period. These data indicate that mouse microglia respond to Degussa P25 with cellular and morphological expressions of free radical formation.

### Introduction

The novel physical and chemical properties of engineered nanoparticles make them attractive for use in medical, agricultural, industrial, manufacturing, and military sectors. Although hundreds of tons of nanoparticles enter the environment annually, little is known of their interactions with biological systems, and recent studies indicate that some are not completely benign to biological and environmental targets (1). Such reports have the potential to transform the focus of environmental protection. The federal government, aware of this possibility, has not only articulated the need for research on the environmental and health effects of nanotechnology (2), but is actively supporting such research (3). Of the many types of nanoproducts in current use, toxicity testing should obviously begin with those that pose the highest risk of environmental exposure (4). Nanosize titanium dioxide (TiO<sub>2</sub>) is a reasonable candidate for study since it is widely used in manufacturing (5, 6), in the environment to decontaminate air, soil, and water (7–11), and more recently in consumer products (e.g., toothpastes, sunscreens, cosmetics, and food products, etc.) (12, 13). Such widespread use and its potential entry through dermal, ingestion, and inhalation routes suggest that nanosize TiO<sub>2</sub> poses considerable exposure risk to humans, livestock, and eco-relevant species (e.g., fish, daphnia, nematodes, and plankton). Although exposure to different TiO<sub>2</sub> particle sizes and formulations (nanosize, pigment grade, and surface coated) has produced only marginal results in rodents (14–16), numerous in vitro studies report that TiO<sub>2</sub> nanoparticles cause oxidative stress (OS)-mediated toxicity in diverse cell types, including human colon cells (17), osteoblasts (18), endothelia (19), epithelia (20), skin fibroblast (21), liver (22), alveolar macrophages (23–25), and *Salmonella* bacteria (26). The potential neurotoxicity of TiO<sub>2</sub> in culture has yet to be examined.

Several studies report that inhaled or injected nanoparticles enter systemic circulation (27–29) and migrate to various organs and tissues, raising concern that they may cause damage to biological systems through OS pathways (30). The brain is especially vulnerable to OS damage, and recent studies indicate that nanosize particles can cross the blood–brain barrier (31) and enter the central nervous system (CNS) of animals (29, 32, 33). In the CNS, OS is largely mediated by the microglia, a macrophage-like, phagocytic cell that is normally inactive unless confronted by potentially damaging, exogenous stimuli (e.g., xenobiotics, chemicals, particles). Their immediate response to such stimuli is known as the "oxidative burst" (34, 35) and involves a rapid sequence of events that includes an increase in metabolic activity, a change in cell shape and size, and cytoplasmic engulfment (i.e., phagocytosis) of the offending stimuli. During phagocytosis, the plasma membrane of the phagocyte surrounds

the foreign substance, invaginates, and internalizes the membrane bound material (i.e., phagosome). The signaling mechanisms for the subsequent oxidative burst are not well defined, but invagination of the plasma membrane appears prerequisite for the activation of a multicomponent enzyme system known as NADPHox and the initiation of the oxidative burst. This activation results in the immediate production of superoxide anions ( $O_2^{\cdot-}$ ) which convert to multiple reactive oxygen species (ROS) including hydrogen peroxide ( $H_2O_2$ ), hydroxyl radicals ( $OH^{\cdot}$ ), and peroxynitrites that can destroy the offending stimuli through OS pathways. The excess  $O_2^{\cdot-}$  and its dismutation product  $H_2O_2$  are either retained within cytoplasmic granules, providing an immediate supply of intracellular oxidants, or allowed to diffuse from the microglial plasma membrane where they can potentially damage the proteins, lipids, and DNA of neighboring cells, especially neurons (36, 37). Microglia-mediated neuronal damage through OS pathways has been proposed to underlie neurodegenerative diseases such as Amyotrophic Lateral Sclerosis, Parkinson's, and Alzheimer's (38–40).

Although the oxidative burst is the major source of ROS in the activated microglia,  $O_2^{\cdot-}$  are also generated as byproducts of normal mitochondrial energy production (i.e., bioenergetics) in the quiescent cell. Mitochondria produce cellular energy (ATP) by transferring electrons along a series of enzymatic complexes (Complex I–IV) known as the Electron Transport Chain (ETC) (41). During this transfer, single electrons escape and reduce molecular oxygen to  $O_2^{\cdot-}$ . This is the fate of approximately 1% of all oxygen consumed and defines the ETC as the major producer of ROS in nonphagocytic cells and tissues. Although, the levels of  $O_2^{\cdot-}$  generated from ETC are relatively low and efficiently neutralized by matrix-located antioxidant enzyme systems (i.e., endogenous scavengers), the rate of  $O_2^{\cdot-}$  generation can be significantly increased if one or more of the ETC enzyme complexes is inhibited.

The  $O_2^{\cdot-}$  formed by the oxidative burst or from ETC leakage is quickly reduced to the more stable  $H_2O_2$  by superoxide dismutase, an enzyme located in intracellular microsomes, peroxisomes, and within the mitochondria matrix. Although  $O_2^{\cdot-}$  radicals can be directly toxic, they have limited reactivity to lipids. However, in the presence of transition metals, most notably ferrous iron, superoxides can convert to the highly reactive hydroxyl radical ( $OH^{\cdot}$ ) via the Fenton reaction. The hydroxyl radical is considered the primary agent of lipid peroxidation.

Several recent articles have prescribed a formal protocol for nanotoxicity testing (4, 42) which suggests that physicochemically described nanoparticles should first be tested in cultures of relevant target cells for the production of ROS. This is followed by toxicity testing in more complex cultures, in eco-relevant species, and ultimately in animals. In the present study, we follow this format by first measuring the ROS response of microglia (BV2) exposed to physicochemically characterized nano-TiO<sub>2</sub> (P25). Microglia were chosen in view of their responsiveness to xenobiotics and their pivotal role in OS-mediated neurodegeneration. The BV2 is an immortalized cell line that responds to pharmaceutical agents, particulates, and environmental chemicals with characteristic signs of OS (43–45). In the present study, BV2 were exposed to noncytotoxic doses of P25, and the immediate and prolonged release of ROS was measured over a 120 min exposure period using various fluoroprobes. Transmission electron microscopy (TEM) was used to document the phagocytic response of the microglia to P25 exposure. Physicochemical properties of P25 (e.g., particle size distribution (PSD), zeta ( $\zeta$ ) potential, and dispersion stability) were measured in culture media and physiological buffer at time points relevant to the biological response.

## Materials and Methods

**Physicochemical Characterization.** Commercial grade, nano-size TiO<sub>2</sub> (Degussa Aeroxide P25) was a gift from Degussa Corp. (Parsippany, NJ) and used without further purification or treatment. Although the physicochemical properties (e.g., particle size distribution,  $\zeta$ -potential, and dispersion stability) of P25 have been previously reported (6, 46, 47), they were remeasured in the present study in the vehicles used to maintain and expose the cell cultures. These included Hank's Basic Salt Solution (HBSS) and Dulbecco's Modified Eagle's Medium (DMEM). Both HBSS and DMEM are high ionic strength solutions with high concentrations of divalent cations that cause P25 to aggregate. DMEM also contains low amounts of glucose and amino acids (Supporting Information, Tables S1, S2). The physicochemical properties of P25 were measured in a slurry prepared from a 1 g/L suspension of P25 in HBSS or DMEM. Slurry concentrations (5–120 ppm) similar to those used to expose cells were used immediately after 1 min sonication. The particle size distribution was measured by dynamic light scattering (Malvern Zeta Sizer Nano ZS, Southborough, MA) over a 3 h period to monitor the growth of the aggregates and to determine a stable aggregate size. For calculating particle size (volume average), the refractive index of the anatase form of TiO<sub>2</sub> ( $n_D = 2.49$ ) (48) was assumed. The  $\zeta$ -potential was determined in both HBSS and DMEM from electrophoretic mobility (EM) measurements of a 30 ppm slurry (Malvern Zeta Sizer Nano ZS, Southborough, MA). The Helmholtz–Smoluchowski equation was used to correlate electrophoretic mobility to  $\zeta$ -potential. The N<sub>2</sub>–BET specific surface area was measured using a Nova 2200e BET surface area analyzer (Quantachrome, Boynton Beach, FL). Samples were degassed in helium for 1 h at 150 °C prior to analysis (49). The dispersion stability, operationally defined as the resistance to sedimentation, was determined by measuring the sedimentation rate of P25 suspensions in HBSS or DMEM. The optical density ( $\lambda = 508$  or 450 nm) of the suspension was monitored for 18 h in a UV–visible spectrophotometer (Varian, Palo Alto, CA). There was a linear relationship between TiO<sub>2</sub> concentration and UV response for all TiO<sub>2</sub> concentrations evaluated.

**Cell Culture Maintenance and Exposure.** BV2 microglia were grown in 225-cm<sup>2</sup> cell culture flasks in DMEM supplemented with 10% Fetal Calf Serum (FCS) and 1% penicillin–streptomycin (ATCC, Manassas, VA). After reaching 85% confluency, cells were transferred to Corning 96-well plates. To minimize light scatter during the spectrophotometric readings, cells were plated in clear-bottom, black (fluorescence), or white (chemiluminescence) 96-well culture plates (Corning Inc., Corning, NY) and examined with a Molecular Devices (Sunnyvale, CA) Spectramax Gemini EM (fluorescence) or Lmax II 384 plate reader (chemiluminescence). Noncytotoxic exposure concentrations were determined from measures of intracellular ATP taken after 1, 6, and 18 h exposure to P25 (2.5–120 ppm) using the CellTiter-Glo assay. For all ROS measurements, P25 was ultrasonicated (~1 min) in 10× stock concentrations in HBSS and exposed to the cells immediately before spectrophotometric readings were taken.

**Probes.** Fluorescent and chemiluminescent probes were chosen to measure the immediate generation of  $H_2O_2$  resulting from the oxidative burst and that resulting from interference with mitochondrial ETC (50). All probes were purchased from Molecular Probes (Eugene, OR) except for the chemiluminescent assay CellTiter-Glo (Promega, Madison, WI). The concentrations and incubation times for each assay were empirically derived and are described in the figure legends. For each fluorescent assay, cells, exposed to the fluorescent probe (i.e., “loaded”), were washed with HBSS to remove any extracellular probe from the cell's external

environment. In this way, only intracellular levels of ROS were measured. Because it has been reported that P25 can be photoactivated by visible light (51), all cell culture procedures (probe “loading”, washings, P25 exposures, etc.) were done under darkroom “safe-lights”.

The production of intracellular H<sub>2</sub>O<sub>2</sub> generated from the oxidative burst was measured at 3 5-min intervals with Image-iT and at 5 15-min intervals with OxyBURST H<sub>2</sub>HFF Green BSA. The production of H<sub>2</sub>O<sub>2</sub> resulting from interference with the mitochondria’s ETC was measured using the mitochondrial specific fluorescent probe MitoSOX at 20-min intervals over a 0–120 min exposure. Changes in the mitochondrial membrane potential, an indicator of the membrane’s net charge, were monitored with MitoTracker Red over 20-min intervals. Data were collected over a 120 min period for each assay. Intracellular levels of ATP, an index of cell viability, were measured at 1, 6, and 18 h postexposure with a luciferase-based chemiluminescence assay, CellTiter-Glo.

**Statistics.** All data were collected using SoftMax Pro 4.8 software (Molecular Devices, Sunnvale, CA). Graphing and statistics were performed with either Excel 2003 (Microsoft, Redmond, WA) or GraphPad Prism 4.02 (GraphPad Software, San Diego, CA). The mean value ( $n = 6$ ) at each concentration was graphed to show a time-course response. At least five time points are depicted for each assay. Data were analyzed using an unpaired two-tailed Student’s *t*-test to determine the lowest statistically significant concentration relative to its unexposed baseline control. The exposure concentration/time point at which a statistically significant difference was observed is indicated on the graphs (\*,  $p \leq 0.05$ ) and described in the figure legends.

**Transmission Electron Microscopy (TEM).** BV2 cells, grown to 85% confluency in 6-well Costar plates (Corning, Inc., Corning, NY), were exposed to P25 particles (2.5 ppm) in 1% reduced serum DMEM for 6 and 18 h. After exposure, cells were washed in warm HBSS to remove all noninternalized particles and fixed overnight in cold 4% cacodylate-buffered glutaraldehyde (Poly Scientific, Bayside NY). Cells were centrifuged (1100 rpm, 5 min) and processed as a pellet for TEM using standard procedures (52). Polymerized blocks were sectioned at 500–700 nm thickness and examined with a Philips CM12 electron microscope.

## Results and Discussion

**Physicochemistry.** The toxicity of nanosize particles has been associated with several physicochemical characteristics, such as the N<sub>2</sub>–BET specific surface area, the  $\zeta$ -potential, and particle aggregate size. These properties were measured in cell culture media (DMEM) and the physiological buffer (HBSS) used to expose the cells. The N<sub>2</sub>–BET specific surface area of P25 was measured at  $52.7 \pm 3.6$  m<sup>2</sup>/g and is consistent with the manufacturer’s data and with previous reports (46, 47, 49, 53). The  $\zeta$ -potentials of P25, measured in DMEM (pH = 7.5) and HBSS (pH = 7.6) were  $-11.6 \pm 1.2$  mV and  $-9.25 \pm 0.73$  mV, respectively. The negative surface charge at physiological pH (pH = 7.5–7.6) was consistent with the commonly reported isoelectric point of  $pH_{IEP} = 6.4$  for Degussa P25 (47, 49, 53).

Degussa P25 is a mixture of the rutile and anatase forms of TiO<sub>2</sub> (70% anatase/30% rutile) with a reported primary crystallite size of ~30 nm (46). P25 rapidly aggregates in both HBSS and DMEM. Both HBSS and DMEM are high osmolarity fluids with approximate ionic strengths of 155 mM and 166 mM, respectively, and both contain high concentrations of the monovalent cations Na<sup>+</sup> and K<sup>+</sup> (160 mM) and the divalent cations Ca<sup>2+</sup> and Mg<sup>2+</sup> (2 mM) as shown in Tables S1 and S2 (Supporting Information). Aggregation continued for 20–45 min after sonication (1 min), until a steady-state stable aggregate size formed (Figure S1). The steady-state

**TABLE 1. Initial and Steady State Particle Geometric Mean Hydrodynamic Diameter for Degussa P25 TiO<sub>2</sub> in HBSS or DMEM<sup>a</sup>**

TiO <sub>2</sub> dose concentration	hydrodynamic diameter (nm)	
	initial	steady-state
5 ppm	500 ± 3 <sup>b</sup>	826 ± 69 <sup>c</sup>
10 ppm	590 ± 3	1164 ± 85
20 ppm	865 ± 32 <sup>d</sup>	1284 ± 57 <sup>d</sup>
30 ppm	992 ± 19	1316 ± 68
80 ppm	1570 ± 20	2090 ± 180
120 ppm	1350 ± 30	2368 ± 163

<sup>a</sup> The chemical composition of HBSS and DMEM is provided in the Supporting Information. <sup>b</sup> Errors represent one standard deviation based on 3 replicate measurements. <sup>c</sup> Average particle size measured after reaching steady state (~30 min). Error bars represent 1 standard deviation of these values. <sup>d</sup> Measured in DMEM.

aggregate size increased from 826 to 2368 nm as the concentration increased from 5 to 120 ppm (Table 1). The size of P25 aggregates was the same in both HBSS and DMEM as these fluids had nearly identical ionic strength and composition. The amino acids and serum present in reduced-serum DMEM (but not in HBSS) did not significantly affect the rate of aggregation or the size of the formed aggregates.

During the 6- and 18-h exposure times described in the TEM studies, BV2 cells (which adhere to the bottom of the cell culture plate/well), were exposed by particle diffusion or sedimentation of aggregates. Such conditions are characteristic of cell culture studies and could produce higher particle exposures than that described by the concentration (54). The sedimentation of P25 aggregates was measured in low serum media at 6- and 18-h exposures to estimate the fraction of particles that settled onto the cells during the TEM exposure (Figure S2). By the end of the 18-h exposure ~20% of the particles remained suspended in reduced serum DMEM. The higher sedimentation rate seen at higher concentrations is consistent with larger sized aggregates formed at the higher test concentrations of P25 (see previous paragraph). A correlation of P25 aggregate size (measured in HBSS) and the concentrations/times needed for significant ROS production is described in the Biological Effects section below.

**Biological Effects.** O<sub>2</sub><sup>•-</sup> is an unstable molecule which is quickly reduced to the more stable and measurable H<sub>2</sub>O<sub>2</sub>. Kinetic analysis of H<sub>2</sub>O<sub>2</sub> production measured both an immediate production of ROS as generated by the oxidative burst (Figure 1A and B) and by a later release caused by disruption of mitochondrial ETC (Figure 2A). Microglia responded to P25 (≥10 ppm) with rapid (<3–5 min) concentration-dependent formation of H<sub>2</sub>O<sub>2</sub> as measured with Image-iT and OxyBURST (Figure 1A and B). In contrast to the rapid increases in H<sub>2</sub>O<sub>2</sub> generated by the oxidative burst (Figure 1A and B), significant release of ROS did not occur until 60 min postexposure (≥20 ppm) as measured by MitoSOX (Figure 2A). MitoTracker Red is a potential-dependent dye. Increases in MitoTracker Red staining intensity indicate increases in the mitochondria’s membrane potential (i.e., hyperpolarization). The fluorescent MitoTracker molecules, which are initially distributed throughout the cytoplasm, accumulate on negatively charged (anionic) membranes. The increased fluorescence suggests a steady exposure concentration-dependent accumulation of net negatively charged O<sub>2</sub><sup>•-</sup> within the mitochondrial membrane (Figure 2B). This plausibly resulted from P25’s inhibition of one or more of the ETC enzymatic complexes (Complex I and III). Depolarization of the mitochondrial membrane is normally associated with a reduction of membrane permeability, an opening of the mitochondrial transition pore, and

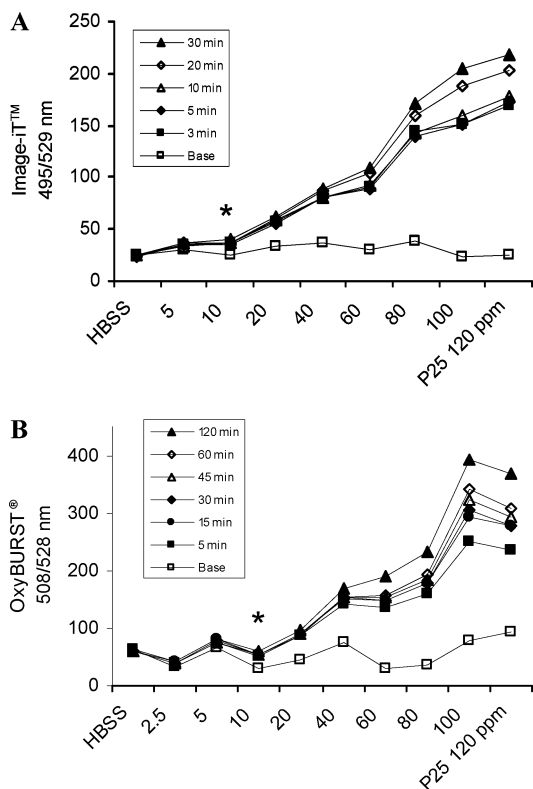


**FIGURE 1.** Extracellular release of  $\text{H}_2\text{O}_2$  was measured using Image-iT and OxyBURST. (A) Cells were incubated (30 min,  $37^\circ\text{C}$ ) in  $25\ \mu\text{M}$  Image-iT + HBSS/ $\text{Ca}^{2+}/\text{Mg}^{2+}$ , washed, and exposed to P25 (5–120 ppm). Significant ( $p < 0.05$ ) increases of fluorescence (measured at 495/529 nm) relative to its baseline occurred in cells exposed to  $\geq 10$  ppm P25 at 3 min, and continued throughout the 30 min recording time. (B) Cells were incubated (30 min,  $37^\circ\text{C}$ ) in  $10\ \mu\text{g}/\text{mL}$  OxyBURST in reduced-serum media, washed, and then exposed to P25 (2.5–120 ppm). Significant ( $p < 0.05$ ) increases of fluorescence (measured at 508/528 nm) occurred in cells exposed to  $\geq 10$  ppm at 5 min and continued to increase throughout the 120 min recording period.

the initiation of necrotic or apoptotic pathways (36, 41). MitoTracker Red did not indicate membrane depolarization in response to P25. This was supported by measures of intracellular ATP (Figure S4) which were maintained at all P25 concentrations throughout the 120 min exposure period, confirming that all cellular expressions of ROS release were measured in actively respiring and viable microglia.

A correlation between the size of P25 aggregates (Figure S2) and the “effective” exposures (i.e., earliest time point and lowest concentration resulting in significant ROS production) was examined. ROS generated from the oxidative burst (Image-iT, OxyBURST) indicated that significant increases occurred at 3–5 min in response to  $\geq 10$  ppm P25. At this time and concentration, P25 aggregate size was  $\sim 750$ – $800$  nm. Significant increases in ROS generated from the mitochondrial ETC occurred  $> 60$  min exposure, in response to  $\geq 20$  ppm P25 as measured with MitoSOX probes. At this time and concentration, P25 aggregate size was  $\sim 1300$  nm. The relationship between “effective” exposures and aggregate size should be routinely measured in nanoparticle toxicity studies since aggregate size can have a profound impact on the cell’s uptake of particles and their response to that uptake.

TEM indicated that after 6 h exposure, P25 aggregates were phagocytized in small clusters and internalized within the microglia’s cytoplasm where they aggregated into electron-dense  $\sim 0.5$ – $2$  micrometer clumps (Figure 3A and B). The appearance of small (100–300 nm) and large

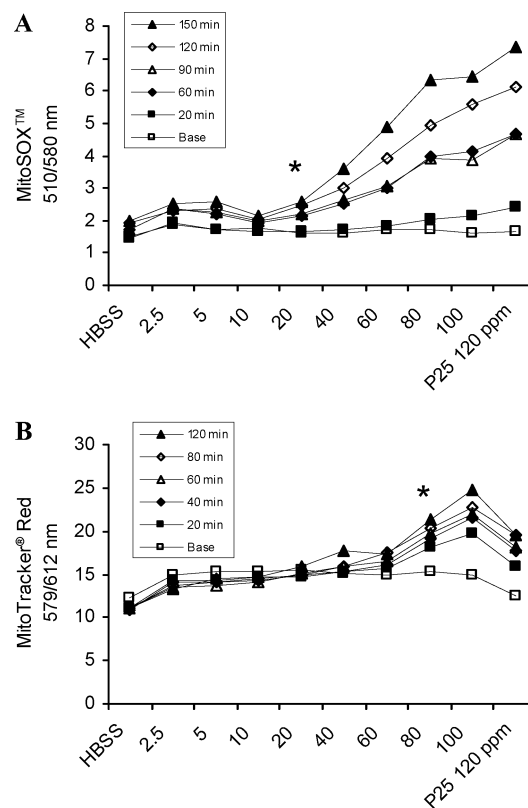


**FIGURE 2.** (A) Increases in  $\text{O}_2^-$  were measured by the fluorescent probe MitoSOX Red. Cells, incubated in  $2\ \mu\text{M}$  MitoSOX (10 min,  $37^\circ\text{C}$ ) showed significant ( $p < 0.05$ ) increases in fluorescence (measured at 510/580 nm) after 60 min exposure to  $\geq 20$  ppm P25, and fluorescence continued to increase for 150 min postexposure. (B) Cells incubated in  $25\ \text{nM}$  MitoTracker Red (20 min,  $37^\circ\text{C}$ ) showed significant ( $p < 0.05$ ) increases in mitochondrial membrane potential (hyper-polarization) relative to its baseline control after 20 min exposure to  $\geq 80$  ppm P25 which continued for  $> 100$  min.

(800–2000 nm) particle aggregates was consistent with the recorded particle size distribution data (Figure S2). Phagocytes (e.g., macrophages, microglia) preferentially engulf particles in the  $1$ – $3\ \mu\text{m}$  range (55). In contrast, nanosize particles ( $< 100$  nm) are not phagocytized in the strict sense, rather, they are engulfed through other, nonspecified mechanisms which involve electrostatic, van der Waals, and steric interactions (56). Ultrastructural evidence of swollen and disrupted mitochondria lying in close proximity to the aggregates of P25 was recorded after 18 h exposure (Figure 3C and D). The appearance of swollen mitochondria suggests that the mitochondrial membrane permeability transition pore has begun to open and apoptotic or necrotic signals initiated (36, 37). Still, the microglia remained viable in response to P25 exposure, since ATP intracellular levels showed no measurable reductions even after 18 h exposures (Figure S4).

In summary, these data demonstrate that nanosize P25 particles stimulate microglia to produce ROS through the oxidative burst and through interference with mitochondrial ETC. Nevertheless, the microglia remained viable at all concentrations of P25, in keeping with their known resistance to ROS damage (38, 57). Whether the microglia’s release of ROS translates into neuronal damage in situ is not addressed in this study, but pilot data indicate that P25 stimulates apoptotic pathways in cultured neurons at concentrations  $> 20$  ppm after 24 h exposure (58). In contrast to earlier reports (59, 60), but in agreement with others (20), photoactivation of P25 does not appear necessary to stimulate ROS in microglia.

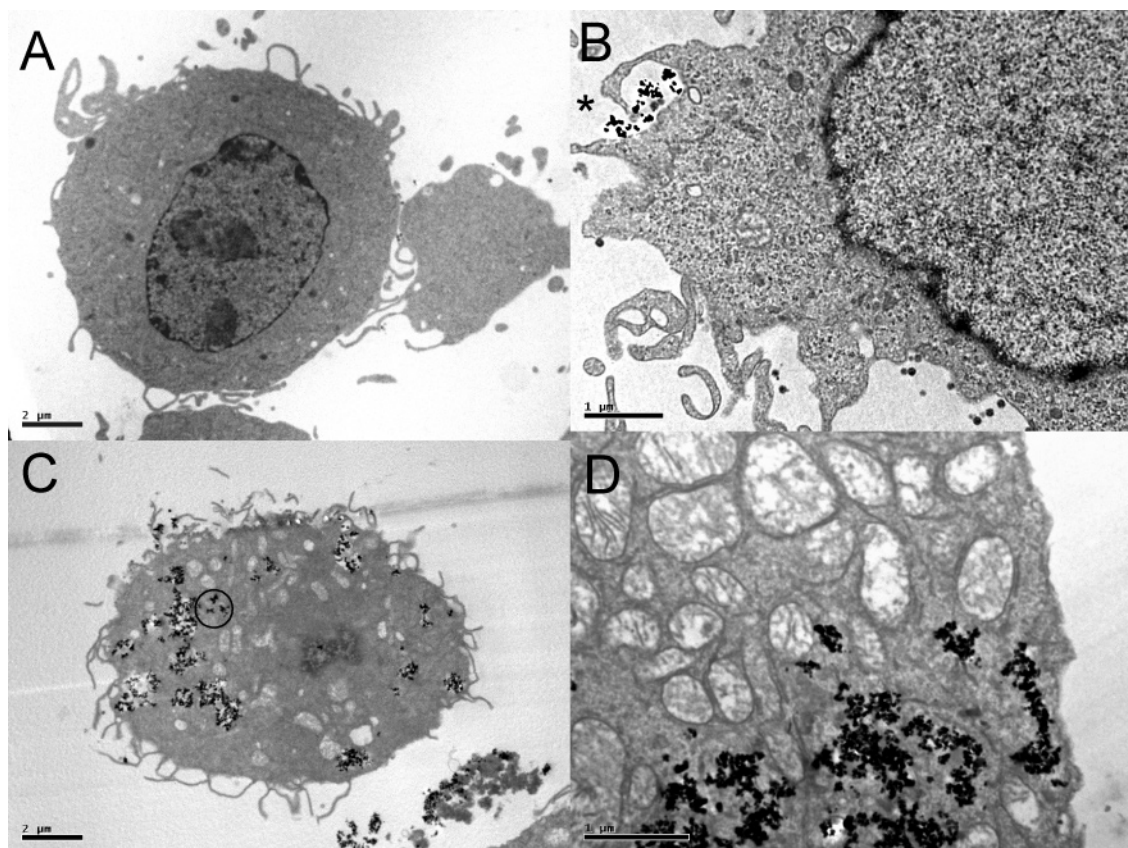


**FIGURE 3.** (A) Quiescent microglia are large, 8–10 micrometer phagocytic cells with many oval-shaped mitochondria visible in their cytoplasm. (B) An early (6 h exposure) response of microglia to 2.5 ppm P25 was the elaboration of numerous pseudopodia which engulfed small groups of electron-dense particles (\*). (C) Within 18 h postexposure, multiple vacuoles containing P25 aggregates were seen in proximity to pale-staining, swollen mitochondria. (D) Higher magnification showed swelling and disruption of mitochondria lying in close proximity to the aggregates. Image magnification: (A) 4400 $\times$ ; (B) 11 400 $\times$ ; (C) 4400 $\times$ ; (D) 18 000 $\times$ .

Certain physical characteristics (e.g., surface charge, size, and surface area) of “incidental” nanosize particles such as airborne particulate matter (PM) are known to influence their toxicity. It is plausible that similar physical properties of engineered nanoparticles could affect biological targets through OS or more novel toxicity pathways (4, 61, 62). Defining the causal mechanism(s) linking those physical properties with their biological effects should be a primary focus of nanotoxicity studies. Studies on the inflammatory toxicity associated with nanosize particulate matter offer some insights into possible mechanisms. Nanosize PM particles appear to mediate toxicity through OS pathways. The pulmonary inflammation associated with their inhalation has been related to the large surface area of the ultrafine particles which exposes a high number of reactive groups on the particle’s surface (42, 63). PM inflammation has also been correlated with the negative surface charge carried by the PM particle (64). Polymodal, sensory receptors embedded in the membrane of microglia and macrophages are possible target sites that could react to negatively charged nanoparticles. For example, the activation of TRPV1 vanilloid sensory receptors by the negative surface charge carried on PM particles stimulates OS inflammatory pathways and the subsequent release of inflammatory cytokines from both respiratory epithelial cells (65) and BV2 microglia (66). Scavenger receptors, found on microglia and macrophages (67), are also sensitive to repeating patterns of charge that may be found on ordered crystalline metal oxide nanoparticles. Such receptors have been implicated in mediating cytotoxicity in alveolar macrophages exposed to TiO<sub>2</sub> (68). In the present study, the negative zeta potential of P25

particles and the ordered arrangement of charged O<sup>-</sup> sites on their surface could be activating either type of receptor and subsequent OS pathways in the microglia. Future studies will examine the causal relationship between the surface charge of nanoparticles and OS mediated events in neurons and other cell types to better understand how the physical properties of particles interact and activate biological systems.

### Acknowledgments

We acknowledge the kind gift of P25 from Degussa Inc. (Parsippany, NJ) and also thank Dr. John Hong, National Institute of Environmental Health Sciences, RTP, NC for the BV2 microglia cell line. We acknowledge the technical support of Martin Schneider, Chapel Hill, NC, and the expert preparation of electron microscopy samples by Wallace Ambrose, School of Dentistry, University of North Carolina, Chapel Hill, NC. This document has been reviewed by the National Health and Environmental Effects Research Laboratory and approved for publication. Approval does not signify that the contents reflect the views of the Agency, nor does mention of trade names or commercial products constitute the endorsement of recommendation for use.

### Supporting Information Available

Additional information on the composition of HBSS and DMEM (Tables S1 and S2) and the physicochemical measurements of P25 (Figures S1–S3); viability data (ATP intracellular measures) taken over an 18 h exposure period (Figure S4). This material is available free of charge via the Internet at <http://pubs.acs.org>.

## Literature Cited

- (1) Oberdörster, E. Manufactured nanomaterials (fullerenes, C<sub>60</sub>) induce oxidative stress in the brain of juvenile largemouth bass. *Environ. Health Perspect.* **2004**, *112*, 1058–1062.
- (2) U.S. House of Representatives, Office of Science. In *Environmental and Safety Impacts of Nanotechnology: What Research is Needed?* 2005; <http://www.house.gov/science/press/109/109-165.htm>.
- (3) Dunphy Guzmán, K. A.; Taylor, M. R.; Banfield, J. F. Environmental risks of nanotechnology: National Nanotechnology Initiative funding, 2000–2004. *Environ. Sci. Technol.* **2006**, *40*, 1401–1407.
- (4) Nel, A.; Xia, T.; Madler, L.; Li, N. Toxic potential of materials at the nanolevel. *Science* **2006**, *311*, 622–627.
- (5) Allen, N. S.; Edge, M.; Sandoval, G.; Verran, J.; Stratton, J.; Maltby, J. Photocatalytic coatings for environmental applications. *Photochem. Photobiol.* **2005**, *81*, 279–290.
- (6) Fisher, J.; Egerton, T. Titanium Compounds, Inorganic. In *Kirk-Othmer Encyclopedia of Chemical Technology*; John Wiley & Sons: New York, 2001.
- (7) Choi, H.; Stathatos, E.; Dionysiou, D. D. Sol–gel preparation of mesoporous photocatalytic TiO<sub>2</sub> films and TiO<sub>2</sub>/Al<sub>2</sub>O<sub>3</sub> composite membranes for environmental applications. *Appl. Catal., B* **2006**, *63*, 60–67.
- (8) Konstantinou, I. K.; Albanis, T. A. TiO<sub>2</sub>-assisted photocatalytic degradation of azo dyes in aqueous solution: kinetic and mechanistic investigations: A review. *Appl. Catal., B* **2004**, *49*, 1–14.
- (9) Balasubramanian, G.; Dionysiou, D. D.; Suidan, M. T.; Baudin, I.; Lainé, J. M. Evaluating the activities of immobilized TiO<sub>2</sub> powder films for the photocatalytic degradation of organic contaminants in water. *Appl. Catal., B* **2004**, *47*, 73–84.
- (10) Esterkin, C. R.; Negro, A. C.; Alfano, O. M.; Cassano, A. E. Air pollution remediation in a fixed bed photocatalytic reactor coated with TiO<sub>2</sub>. *AIChE J.* **2005**, *51*, 2298–2310.
- (11) Higarashi, M. M.; Jardim, W. F. Remediation of pesticide contaminated soil using TiO<sub>2</sub> mediated by solar light. *Catal. Today* **2002**, *76*, 201–207.
- (12) Wolf, R.; Matz, H.; Orion, E.; Lipozencic, J. Sunscreens—the ultimate cosmetic. *Acta Dermatovenerol. Croat.* **2003**, *11*, 158–162.
- (13) Kaida, T.; Kobayashi, K.; Adachi, M.; Suzuki, F. Optical characteristics of titanium oxide interference film and the film laminated with oxides and their applications for cosmetics. *J. Cosmet. Sci.* **2004**, *55*, 219–220.
- (14) Bermudez, E.; Mangum, J. B.; Wong, B. A.; Asgharian, B.; Hext, P. M.; Warheit, D. B.; Everitt, J. I. Pulmonary responses of mice, rats, and hamsters to subchronic inhalation of ultrafine titanium dioxide particles. *Toxicol. Sci.* **2004**, *77*, 347–357.
- (15) Oberdörster, G.; Finkelstein, J. N.; Johnston, C.; Gelein, R.; Cox, C.; Baggs, R.; Elder, A. C. Acute pulmonary effects of ultrafine particles in rats and mice. *Res. Rep. Health Eff. Inst.* **2000**, *96*, 5–74.
- (16) Warheit, D. B.; Brock, W. J.; Lee, K. P.; Webb, T. R.; Reed, K. L. Comparative pulmonary toxicity inhalation and instillation studies with different TiO<sub>2</sub> particle formulations: impact of surface treatments on particle toxicity. *Toxicol. Sci.* **2005**, *88*, 514–524.
- (17) Zhang, A. P.; Sun, Y. P. Photocatalytic killing effect of TiO<sub>2</sub> nanoparticles on Ls-174-t human colon carcinoma cells. *World J. Gastroenterol.* **2004**, *10*, 3191–3193.
- (18) Ramires, P. A.; Romito, A.; Cosentino, F.; Milella, E. The influence of titania/hydroxyapatite composite coatings on in vitro osteoblasts behaviour. *Biomaterials* **2001**, *22*, 1467–1474.
- (19) Peters, K.; Unger, R. E.; Kirkpatrick, C. J.; Gatti, A. M.; Monari, E. Effects of nanoscaled particles on endothelial cell function in vitro: studies on viability, proliferation and inflammation. *J. Mater. Sci. Mater. Med.* **2004**, *15*, 321–325.
- (20) Gurr, J.-R.; Wang, A. S.; Chen, C.-H.; Jan, K.-Y. Ultrafine titanium dioxide particles in the absence of photoactivation can induce oxidative damage to human bronchial epithelial cells. *Toxicology* **2005**, *213*, 66–73.
- (21) Wamer, W. G.; Yin, J. J.; Wei, R. R. Oxidative damage to nucleic acids photosensitized by titanium dioxide. *Free Radical Biol. Med.* **1997**, *23*, 851–858.
- (22) Hussain, S. M.; Hess, K. L.; Gearhart, J. M.; Geiss, K. T.; Schlager, J. J. In vitro toxicity of nanoparticles in BRL 3A rat liver cells. *Toxicol. In Vitro* **2005**, *19*, 975–983.
- (23) Renwick, L. C.; Donaldson, K.; Clouter, A. Impairment of alveolar macrophage phagocytosis by ultrafine particles. *Toxicol. Appl. Pharmacol.* **2001**, *172*, 119–127.
- (24) Afaq, F.; Abidi, P.; Matin, R.; Rahman, Q. Cytotoxicity, pro-oxidant effects and antioxidant depletion in rat lung alveolar macrophages exposed to ultrafine titanium dioxide. *J. Appl. Toxicol.* **1998**, *18*, 307–312.
- (25) Beck-Speier, I.; Dayal, N.; Karg, E.; Maier, K. L.; Roth, C.; Ziesenis, A.; Heyder, J. Agglomerates of ultrafine particles of elemental carbon and TiO<sub>2</sub> induce generation of lipid mediators in alveolar macrophages. *Environ. Health Perspect.* **2001**, *109 Suppl 4*, 613–618.
- (26) Nakagawa, Y.; Wakuri, S.; Sakamoto, K.; Tanaka, N. The photogenotoxicity of titanium dioxide particles. *Mutat. Res.* **1997**, *394*, 125–132.
- (27) Takenaka, S.; Karg, E.; Roth, C.; Schulz, H.; Ziesenis, A.; Heinzmann, U.; Schramel, P.; Heyder, J. Pulmonary and systemic distribution of inhaled ultrafine silver particles in rats. *Environ. Health Perspect.* **2001**, *109*, 547–551.
- (28) Nemmar, A.; Hoet, P. H.; Vanquickenborne, B.; Dinsdale, D.; Thomeer, M.; Hoylaerts, M. F.; Vanbilloen, H.; Mortelmans, L.; Nemery, B. Passage of inhaled particles into the blood circulation in humans. *Circulation* **2002**, *105*, 411–414.
- (29) Meiring, J. J.; Borm, P. J.; Bagate, K.; Semmler, M.; Seitz, J.; Takenaka, S.; Kreyling, W. G. The influence of hydrogen peroxide and histamine on lung permeability and translocation of iridium nanoparticles in the isolated perfused rat lung. *Part. Fibre Toxicol.* **2005**, *2*, 3.
- (30) Samet, J. M.; DeMarini, D. W.; Malling, H. V. Do airborne particles induce heritable mutations? *Science* **2004**, *304*, 971–972.
- (31) Lockman, P.; Oyewumi, M.; Koziara, J.; Roder, K.; Mumper, R.; Allen, D. Brain uptake of thiamine-coated nanoparticles. *J. Controlled Release* **2003**, *93*, 271–282.
- (32) Kreyling, W. G.; Semmler, M.; Erbe, F.; Mayer, P.; Takenaka, S.; Schulz, H.; Oberdörster, G.; Ziesenis, A. Translocation of ultrafine insoluble iridium particles from lung epithelium to extrapulmonary organs is size dependent but very low. *J. Toxicol. Environ. Health A* **2002**, *65*, 1513–1530.
- (33) Oberdörster, G.; Sharp, Z.; Atudorei, V.; Elder, A.; Gelein, R.; Kreyling, W.; Cox, C. Translocation of inhaled ultrafine particles to the brain. *Inhal. Toxicol.* **2004**, *16*, 437–445.
- (34) Colton, C. A.; Gilbert, D. L. Production of superoxide anions by a CNS macrophage, the microglia. *FEBS Lett.* **1987**, *223*, 284–288.
- (35) Segal, A. W.; Abo, A. The biochemical basis of the NADPH oxidase of phagocytes. *Trends Biochem. Sci.* **1993**, *18*, 43–47.
- (36) De Giorgi, F.; Lartigue, L.; Bauer, M. K.; Schubert, A.; Grimm, S.; Hanson, G. T.; Remington, S. J.; Youle, R. J.; Ichas, F. The permeability transition pore signals apoptosis by directing Bax translocation and multimerization. *FASEB J.* **2002**, *16*, 607–609.
- (37) Fernandes, M. A.; Santos, M. S.; Vicente, J. A.; Moreno, A. J.; Vেলা, A.; Duburs, G.; Oliveira, C. R. Effects of 1,4-dihydropyridine derivatives (cerebrocrast, gammapyrone, glutapyrone, and diethone) on mitochondrial bioenergetics and oxidative stress: a comparative study. *Mitochondrion* **2003**, *3*, 47–59.
- (38) Block, M. L.; Hong, J. S. Microglia and inflammation-mediated neurodegeneration: multiple triggers with a common mechanism. *Prog. Neurobiol.* **2005**, *76*, 77–98.
- (39) Colton, C. A.; Chernyshev, O. N.; Gilbert, D. L.; Vitek, M. P. Microglial contribution to oxidative stress in Alzheimer's disease. *Ann. N. Y. Acad. Sci.* **2000**, *899*, 292–307.
- (40) Liu, B.; Hong, J. S. Role of microglia in inflammation-mediated neurodegenerative diseases: mechanisms and strategies for therapeutic intervention. *J. Pharmacol. Exp. Ther.* **2003**, *304*, 1–7.
- (41) Fariss, M. W.; Chan, C. B.; Patel, M.; Van, H. B.; Orrenius, S. Role of mitochondria in toxic oxidative stress. *Mol. Interventions* **2005**, *5*, 94–111.
- (42) Oberdörster, G.; Maynard, A.; Donaldson, K.; Castranova, V.; Fitzpatrick, J.; Ausman, K.; Carter, J.; Karn, B.; Kreyling, W.; Lai, D.; Olin, S.; Monteiro-Riviere, N.; Warheit, D.; Yang, H. Principles for characterizing the potential human health effects from exposure to nanomaterials: elements of a screening strategy. *Part. Fibre Toxicol.* **2005**, *2*, 8.
- (43) Block, M. L.; Wu, X.; Pei, Z.; Li, G.; Wang, T.; Qin, L.; Wilson, B.; Yang, J.; Hong, J. S.; Veronesi, B. Nanometer size diesel exhaust particles are selectively toxic to dopaminergic neurons: the role of microglia, phagocytosis, and NADPH oxidase. *FASEB J.* **2004**, *18*, 1618–1620.
- (44) Wu, X. F.; Block, M. L.; Zhang, W.; Qin, L.; Wilson, B.; Zhang, W. Q.; Veronesi, B.; Hong, J. S. The role of microglia in paraquat-induced dopaminergic neurotoxicity. *Antioxid. Redox Signaling* **2005**, *7*, 654–661.

- (45) Shafer, L. L.; McNulty, J. A.; Young, M. R. Brain activation of monocyte lineage cells: brain-derived soluble factors differentially regulate BV2 microglia and peripheral macrophage immune functions. *Neuroimmunomodulation* **2002**, *10*, 283–294.
- (46) Kirchnerova, J.; Herrera Cohen, M.-L.; Guy, C.; Klvana, D. Photocatalytic oxidation of *n*-butanol under fluorescent visible light lamp over commercial TiO<sub>2</sub> (Hombicat UV100 and Degussa P25). *Appl. Catal. A* **2005**, *282*, 321–332.
- (47) Dionysiou, D. D.; Suidan, M. T.; Bekoua, E.; Baudin, I.; Láiné, J.-M. Effect of ionic strength and hydrogen peroxide on the photocatalytic degradation of 4-chlorobenzoic acid in water. *Appl. Catal. B* **2000**, *26*, 153–171.
- (48) Lide, D. *CRC Handbook of Chemistry and Physics*; CRC Press: Boca Raton, FL, 2005.
- (49) Dutta, P. K.; Ray, A. K.; Sharma, V. K.; Millero, F. J. Adsorption of arsenate and arsenite on titanium dioxide suspensions. *J. Colloid Interface Sci.* **2004**, *278*, 270–275.
- (50) Generating and detecting reactive oxygen species. In *The Handbook – A Guide to Fluorescent Probes and Labeling Technologies*; Invitrogen Corporation: Carlsbad, CA, 2005; Chapter 18.2.
- (51) Hurum, D. C.; Agrios, A. G.; Gray, K. A.; Rajh, T.; Thurnauer, M. Explaining the enhanced photocatalytic activity of Degussa P25 mixed-phase TiO<sub>2</sub> using EPR. *J. Phys. Chem. B* **2003**, *107*, 4545–4549.
- (52) Phillips, D. M. Electron microscopy: use of transmission and scanning electron microscopy to study cells in culture. *Methods Cell Biol.* **1998**, *57*, 297–311.
- (53) Ferguson, M. A.; Hoffmann, M. R.; Hering, J. G. TiO<sub>2</sub>-photocatalyzed As(III) oxidation in aqueous suspensions: reaction kinetics and effects of adsorption. *Environ. Sci. Technol.* **2005**, *39*, 1880–1886.
- (54) Limbach, L. K.; Li, Y.; Grass, R. N.; Brunner, T. J.; Hintermann, M. A.; Muller, M.; Gunther, D.; Stark, W. J. Oxide nanoparticle uptake in human lung fibroblasts: effects of particle size, agglomeration, and diffusion at low concentrations. *Environ. Sci. Technol.* **2005**, *39*, 9370–9376.
- (55) Geiser, M. Morphological aspects of particle uptake by lung phagocytes. *Microsc. Res. Technol.* **2002**, *57*, 512–522.
- (56) Rimai, D. S.; Quesnel, D. J.; Busnaia, A. A. The adhesion of dry particles in the nanometer to micrometer-size range. *Colloids Surf., A* **2000**, *165*, 3–10.
- (57) Emerit, J.; Edeas, M.; Bricaire, F. Neurodegenerative diseases and oxidative stress. *Biomed. Pharmacother.* **2004**, *58*, 39–46.
- (58) Long, T.; Saleh, N.; Phenrat, T.; Swartz, C.; Parker, J.; Lowry, G. V.; Veronesi, B. Metal oxide nanoparticles produce oxidative stress in CNS microglia and neurons: physicochemical, cellular and genomic analysis. *The Toxicologist* **2006**, *75*.
- (59) Nagaveni, K.; Hegde, M. S.; Ravishankar, N.; Subbanna, G. N.; Madras, G. Synthesis and structure of nanocrystalline TiO<sub>2</sub> with lower band gap showing high photocatalytic activity. *Langmuir* **2004**, *20*, 2900–2907.
- (60) Uchino, T.; Tokunaga, H.; Ando, M.; Utsumi, H. Quantitative determination of OH radical generation and its cytotoxicity induced by TiO(2)–UVA treatment. *Toxicol. In Vitro* **2002**, *16*, 629–635.
- (61) Kreyling, W. G.; Semmler, M.; Möller, W. Dosimetry and toxicology of ultrafine particles. *J. Aerosol Med.* **2004**, *17*, 140–152.
- (62) Donaldson, K.; Stone, V. Current hypotheses on the mechanisms of toxicity of ultrafine particles. *Ann. Ist. Super. Sanita.* **2003**, *39*, 405–410.
- (63) Renwick, L. C.; Brown, D.; Clouter, A.; Donaldson, K. Increased inflammation and altered macrophage chemotactic responses caused by two ultrafine particle types. *Occup. Environ. Med.* **2004**, *61*, 442–447.
- (64) Veronesi, B.; de Haar, C.; Lee, L.; Oortgiesen, M. The surface charge of visible particulate matter predicts biological activation in human bronchial epithelial cells (BEAS-2B). *Toxicol. Appl. Pharmacol.* **2002**, *178*, 144–154.
- (65) Veronesi, B.; Oortgiesen, M. Neurogenic inflammation and particulate matter (PM) air pollutants. *Neurotoxicology* **2001**, *22*, 795–810.
- (66) Pooler, M.; Makwana, O.; Carter, J.; Beck-Speier I.; Kreyling W.; Veronesi, B. Electrostatic charge on nanoparticles activates CNS macrophages (microglia). *The Toxicologist CD—An Official Journal of the Society of Toxicology* **2005**, *84*.
- (67) Husemann, J.; Loike, J. D.; Anankov, R.; Febbraio, M.; Silverstein, S. C. Scavenger receptors in neurobiology and neuropathology: their role on microglia and other cells of the nervous system. *Glia* **2002**, *40*, 195–205.
- (68) Kim, J. K.; Lee, W. K.; Lee, E. J.; Cho, Y. J.; Lee, K. H.; Kim, H. S.; Chung, Y.; Kim, K. A.; Lim, Y. Mechanism of silica- and titanium dioxide-induced cytotoxicity in alveolar macrophages. *J. Toxicol. Environ. Health A* **1999**, *58*, 437–450.

Received for review March 13, 2006. Revised manuscript received April 28, 2006. Accepted May 3, 2006.

ES060589N